bioRxiv preprint doi: https://doi.org/10.1101/2020.03.09.983247. this version posted March 12, 2020. The copyright holder for this preprint (which was not certified by peer review) is the author/funder. All rights reserved. No reuse allowed without permission.

1 **Inhibition of SARS-CoV-2 infection (previously 2019-nCoV) by a highly potent**
2 **pan-coronavirus fusion inhibitor targeting its spike protein that harbors a high**
3 **capacity to mediate membrane fusion**

4 Shuai Xia,[1#] Meiqin Liu,[2,8#] Chao Wang,[4#] Wei Xu,[1#] Qiaoshuai Lan,[1] Siliang Feng[4],
5 Feifei Qi,[5] Linlin Bao,[5] Lanying Du,[6] Shuwen Liu,[7] Chuan Qin,[5] Fei Sun[3]*, Zhengli
6 Shi[2]*, Yun Zhu,[3]*, Shibo Jiang,[1,6]* Lu Lu[1]*

7 [1]Key Laboratory of Medical Molecular Virology (MOE/NHC/CAMS), School of
8 Basic Medical Sciences, Fudan-Jinbo Joint Research Center, Fudan University,
9 Shanghai, China;

10 [2]CAS Key Laboratory of Special Pathogens, Wuhan Institute of Virology, Center for
11 Biosafety Mega-Science, Chinese Academy of Sciences, Wuhan, China;

12 [3]National Laboratory of Biomacromolecules, Institute of Biophysics, Chinese
13 Academy of Sciences, Beijing, China;

14 [4]State Key Laboratory of Toxicology and Medical Countermeasures, Beijing Institute
15 of Pharmacology and Toxicology, 27 Tai-Ping Road, Beijing 100850, China;

16 [5]Key Laboratory of Human Disease Comparative Medicine, Chinese Ministry of
17 Health, Beijing Key Laboratory for Animal Models of Emerging and Re-emerging
18 Infectious Diseases, Institute of Laboratory Animal Science, Chinese Academy of
19 Medical Sciences and Comparative Medicine Center, Peking Union Medical College,
20 Beijing 100021, China;

21 [6]Lindsley F. Kimball Research Institute, New York Blood Center, New York, NY,
22 USA;

23 [7]Guangdong Provincial Key Laboratory of New Drug Screening, Guangzhou Key
24 Laboratory of Drug Research for Emerging Virus Prevention and Treatment, School of
25 Pharmaceutical Sciences, Southern Medical University, Guangzhou, China;

26 [8]University of Chinese Academy of Sciences, Beijing, People's Republic of China.

27 [#]Contributed equally

bioRxiv preprint doi: https://doi.org/10.1101/2020.03.09.983247. this version posted March 12, 2020. The copyright holder for this preprint (which was not certified by peer review) is the author/funder. All rights reserved. No reuse allowed without permission.

28 *Correspondence to: feisun@ibp.ac.cn, zlshi@wh.iov.cn, zhuyun@ibp.ac.cn,
29 shibojiang@fudan.edu.cn or lul@fudan.edu.cn

bioRxiv preprint doi: https://doi.org/10.1101/2020.03.09.983247. this version posted March 12, 2020. The copyright holder for this preprint (which was not certified by peer review) is the author/funder. All rights reserved. No reuse allowed without permission.

30 **Abstract**

31 The recent outbreak of coronavirus disease (COVID-19) caused by SARS-CoV-2
32 infection in Wuhan, China has posed a serious threat to global public health. To
33 develop specific anti-coronavirus therapeutics and prophylactics, the molecular
34 mechanism that underlies viral infection must first be confirmed. Therefore, we herein
35 used a SARS-CoV-2 spike (S) protein-mediated cell-cell fusion assay and found that
36 SARS-CoV-2 showed plasma membrane fusion capacity superior to that of
37 SARS-CoV. We solved the X-ray crystal structure of six-helical bundle (6-HB) core
38 of the HR1 and HR2 domains in SARS-CoV-2 S protein S2 subunit, revealing that
39 several mutated amino acid residues in the HR1 domain may be associated with
40 enhanced interactions with HR2 domain. We previously developed a pan-coronavirus
41 fusion inhibitor, EK1, which targeted HR1 domain and could inhibit infection by
42 divergent human coronaviruses tested, including SARS-CoV and MERS-CoV. We
43 then generated a series of lipopeptides and found that the EK1C4 was the most potent
44 fusion inhibitor against SARS-CoV-2 S protein-mediated membrane fusion and
45 pseudovirus infection with IC_{50}s of 1.3 and 15.8 nM, about 241- and 149-fold more
46 potent than that of EK1 peptide, respectively. EK1C4 was also highly effective
47 against membrane fusion and infection of other human coronavirus pseudoviruses
48 tested, including SARS-CoV and MERS-CoV, as well as SARSr-CoVs, potently
49 inhibiting replication of 4 live human coronaviruses, including SARS-CoV-2.
50 Intranasal application of EK1C4 before or after challenge with HCoV-OC43 protected
51 mice from infection, suggesting that EK1C4 could be used for prevention and
52 treatment of infection by currently circulating SARS-CoV-2 and emerging
53 SARSr-CoVs.

54 **Keywords:** Coronavirus; SARS-CoV; SARS-CoV-2; 2019-nCoV; fusion inhibitor

bioRxiv preprint doi: https://doi.org/10.1101/2020.03.09.983247. this version posted March 12, 2020. The copyright holder for this preprint (which was not certified by peer review) is the author/funder. All rights reserved. No reuse allowed without permission.

55 **Introduction**

56 In April of 2018, the World Health Organization (WHO) established a priority
57 list of pathogens, including Middle East respiratory syndrome (MERS), severe acute
58 respiratory syndrome (SARS) and Disease X, a disease with an epidemic or pandemic
59 potential caused by an unknown pathogen[1,2] (Fig.1a).

60 In late December 2019, an outbreak of pneumonia with an unknown etiology in
61 Wuhan, China was considered as the first Disease X following the announcement by
62 WHO. Shortly thereafter, a novel coronavirus, 2019-nCoV, as denoted by WHO [3],
63 was identified as the pathogen causing the coronavirus disease COVID-19 [4,5].
64 2019-nCoV with 79.5% and 96% sequence identity to SARS-CoV and a bat
65 coronavirus, SL-CoV-RaTG13, respectively [6], was renamed SARS-CoV-2 by the
66 Coronaviridae Study Group (CSG) of the International Committee on Taxonomy of
67 Viruses (ICTV) [7], while, in the interim, it was renamed HCoV-19, as a common virus
68 name, by a group of virologists in China [8-10].

69 As of 24 February 2020, a total of 79,331 confirmed cases of COVID-19,
70 including 2,618 deaths, were reported in China and 27 other countries [11], posing a
71 serious threat to global public health and thus calling for the prompt development of
72 specific anti-coronavirus therapeutics and prophylactics for treatment and prevention
73 of COVID-19.

74 Coronaviruses (CoVs), the largest RNA viruses identified so far, belonging to the
75 *Coronaviridae* family, are divided into 4 genera, α-, β-, δ- and γ-coronaviruses, while
76 the β-coronaviruses are further divided into A, B, C, and D lineages. The seven CoVs
77 that can infect humans (HCoVs) include HCoV-229E and HCoV-NL63 in the
78 α-coronaviruses, HCoV-OC43 and HCoV-HKU1 in the β-coronaviruses lineage A,
79 SARS-CoV and SARS-CoV-2 in the β-coronaviruses lineage B (β-B coronaviruses),
80 and MERS-CoV in the β-coronaviruses lineage C [6]. To develop specific SARS-CoV-2
81 fusion inhibitors, it is essential to study the fusion capacity of SARS-CoV-2 compared
82 to that of SARS-CoV. Particularly, the spike (S) protein S2 subunit of SARS-CoV-2,

bioRxiv preprint doi: https://doi.org/10.1101/2020.03.09.983247. this version posted March 12, 2020. The copyright holder for this preprint (which was not certified by peer review) is the author/funder. All rights reserved. No reuse allowed without permission.

83 which mediates membrane fusion, has 89.8% sequence identity and 96.9% sequence
84 similarity to those of SARS-CoV, and both of them utilize human
85 angiotensin-converting enzyme 2 (hACE2) as the receptor to infect human cells [6].
86 Most importantly, the ACE2-binding affinity of the receptor-binding domain (RBD) in
87 S1 subunit of S protein of SARS-CoV-2 is 10- to 20-fold higher than that of
88 SARS-CoV [12], which may contribute to the higher infectivity and transmissibility of
89 SARS-CoV-2 compared to SARS-CoV. However, it is unclear whether SARS-CoV-2
90 can mediate membrane fusion in a manner that exceeds the capacity of SARS-CoV.

91 After binding of RBD in S1 subunit of S protein on the virion to the ACE2
92 receptor on the target cell, the heptad repeat 1 (HR1) and 2 (HR2) domains in its S2
93 subunit of S protein interact with each other to form a six-helix bundle (6-HB) fusion
94 core, bringing viral and cellular membranes into close proximity for fusion and
95 infection [13]. Therefore, the 6-HB fusion core structure of SARS-CoV-2 and
96 SARS-CoV S proteins should also be compared in order to investigate the structural
97 basis for membrane fusion mediated by their S proteins and thus set the stage for the
98 rational design of coronavirus fusion inhibitors.

99 In our previous studies, we designed a pan-coronavirus fusion inhibitor, EK1,
100 targeting the HR1 domains of HCoV S proteins, which proved to be effective in
101 inhibiting infection of 5 HCoVs, including SARS-CoV and MERS-CoV, and 3
102 SARS-related CoVs (SARSr-CoVs). By intranasal application of this peptide, either
103 pre- or post-challenge with a coronavirus, the treated mice were protected from
104 HCoV-OC43 or MERS-CoV infection, suggesting that this peptide has prophylactic
105 and therapeutic potential against SARS-CoV-2 infection[14]. Indeed, our recent studies
106 have shown that EK1 peptide is effective against SARS-CoV-2 S protein-mediated
107 membrane fusion and PsV infection in a dose-dependent manner [15].

108 In this study, we have shown that SARS-CoV-2 exhibits much higher capacity of
109 membrane fusion than SARS-CoV, suggesting that the fusion machinery of
110 SARS-CoV-2 is an important target for development of coronavirus fusion inhibitors.

bioRxiv preprint doi: https://doi.org/10.1101/2020.03.09.983247. this version posted March 12, 2020. The copyright holder for this preprint (which was not certified by peer review) is the author/funder. All rights reserved. No reuse allowed without permission.

111 We have solved the X-ray crystal structure of SARS-CoV-2's 6-HB core and
112 identified several mutated amino acid residues in HR1 domain responsible for its
113 enhanced interactions with HR2 domain. By conjugating the cholesterol molecule to
114 the EK1 peptide, we found that one of the lipopeptides, EK1C4, exhibited highly
115 potent inhibitory activity against SARS-CoV-2 S-mediated membrane fusion and PsV
116 infection, about 240- and 150-fold more potent than EK1 peptide, respectively.
117 EK1C4 is also highly effective against *in vitro* and *in vivo* infection of some live
118 HCoVs, such as SARS-CoV-2, HCoV-OC43 and MERS-CoV, suggesting potential for
119 further development as pan-CoV fusion inhibitor-based therapeutics and prophylactics
120 for treatment and prevention of infection by the currently circulating SARS-CoV-2
121 and MERS-CoV, as well as future reemerging SARS-CoV and emerging
122 SARSr-CoVs.

123 **Results**

124 **The capacity of SARS-CoV-2 S protein-mediated membrane fusion**

125 From the GISAID Platform (https://platform.gisaid.org), we obtained the
126 full-length amino-acid sequence of SARS-CoV-2 (BetaCoV 2019-2020) S protein
127 (GenBank: QHD43416). Through alignment with SARS-CoV and SL-CoVs S
128 proteins, we located the functional domains in SARS-CoV-2 S protein, which
129 contains S1 subunit and S2 subunit with the cleavage site at R685/S686 [15]. S1 subunit
130 is located within the N-terminal 14–685 amino acids of S protein, containing
131 N-terminal domain (NTD), receptor binding domain (RBD), and receptor binding
132 motif (RBM). S2 subunit contains fusion peptide (FP), heptad repeat 1 (HR1), heptad
133 repeat 2 (HR2), transmembrane domain (TM) and cytoplasmic domain (CP) (Fig. 1b).

134 Recent biophysical and structural evidence showed that SARS-CoV-2 S protein
135 binds hACE2 with 10-fold to 20-fold higher affinity than SARS-CoV S protein,
136 suggesting the higher infectivity of the new virus [12]. Unlike other β-B coronaviruses,
137 S protein of SARS-CoV-2 harbors a special S1/S2 furin-recognizable site, indicating
138 that its S protein might possess some unique infectious properties. Indeed, in live

bioRxiv preprint doi: https://doi.org/10.1101/2020.03.09.983247. this version posted March 12, 2020. The copyright holder for this preprint (which was not certified by peer review) is the author/funder. All rights reserved. No reuse allowed without permission.

139 SARS-CoV-2 infection, we found a typical syncytium phenomenon naturally formed
140 by infected cells, which is rarely reported in SARS-CoV infection (Fig. 1c). To
141 further explore the special characteristic of SARS-CoV-2 infection, we cloned the S
142 gene into PAAV-IRES-GFP vector and established the S-mediated cell-cell fusion
143 system, using 293T cells that express SARS-CoV-2 S protein and EGFP
144 (293T/SARS-CoV-2/EGFP) as the effector cells, and ACE2/293T cells expressing
145 human ACE2 receptor as the target cells (Fig. 1d and Fig. S1a). After effector cells
146 and target cells were cocultured at 37 °C for 2 h, the fused cells showed at least 2-fold
147 larger size than normal cells and multiple nuclei, and these cells were observed in the
148 SARS-CoV-2 group, but not the SARS-CoV group. After coincubation for 24 h,
149 hundreds of target cells fused together as one big syncytium, containing multiple
150 nuclei (Fig. 1d). Another 24h later, the syncytium grew bigger and could be easily
151 observed under both light and fluorescence microscopy (Fig. 1e). Similar results were
152 observed in the fusion between 293T/SARS-CoV-2/EGFP cells and Huh-7 cells,
153 which naturally express human ACE2 receptor on the cell surface. Their syncytium
154 was obviously formed after coincubation for 48 h, similar to the syncytium formed by
155 live SARS-CoV-2-infected Huh-7 cells (Fig. 1c and 1f). On the contrary, SARS-CoV
156 S protein lacked the ability to mediate the cell-cell fusion under the same conditions
157 (Fig. 1d) based on the required presence of exogenous trypsin to complete membrane
158 fusion in our previous studies. Therefore, compared to SARS-CoV, SARS-CoV-2 S
159 protein showed much more efficiency in mediating viral surface-fusion and entry into
160 target cells [14]. Meanwhile, no fusion was observed for 293T/EGFP cells without
161 S-expression or 293T cells without ACE2-expression (Fig. 1d and Fig. S1b),
162 confirming that S-receptor engagement is necessary for the S-mediated viral fusion
163 and entry.

164 **X-ray crystallographic analysis of the 6-HB fusion core formed by HR1 and HR2**
165 **domains in S2 subunit of SARS-CoV-2 S protein**

166 Previously, we identified that the 6-HB formed by HR1 and HR2 domains of the

bioRxiv preprint doi: https://doi.org/10.1101/2020.03.09.983247. this version posted March 12, 2020. The copyright holder for this preprint (which was not certified by peer review) is the author/funder. All rights reserved. No reuse allowed without permission.

167 S2 subunit plays a very important role in the membrane fusion process mediated by
168 MERS-CoV or SARS-CoV S protein [16,17]. Similarly, our recent study suggested that
169 HR1 and HR2 in subunit S2 of SARS-CoV-2 also interacted to form coiled-coil
170 complex to support membrane fusion and viral infection[15] (Fig. 2a and Fig. S2).
171 However, the specific binding characteristics of SARS-CoV-2 6-HB remained to be
172 explored.

173 To understand the structural basis of the interactions between HR1 and HR2
174 regions of SARS-CoV-2, a fusion protein containing the major parts of HR1 (residues
175 910 to 988) and HR2 (residues 1162 to 1206) with a flexible linker (L6, SGGRGG) in
176 between was constructed for crystallographic study. The crystal structure of
177 HR1-L6-HR2 shows a canonical 6-HB structure with a rod-like shape 115 Å in length
178 and 25 Å in diameter (Fig. 2b). The three HR1 domains form a parallel trimeric
179 coiled-coil center, around which three HR2 domains are entwined in an antiparallel
180 manner. The interaction between these two domains is predominantly a hydrophobic
181 force. Each pair of two adjacent HR1 helices forms a deep hydrophobic groove,
182 providing the binding site for hydrophobic residues of the HR2 domain, including
183 V1164, L1166, I1169, I1172, A1174, V1176, V1177, I1179, I1183, L1186, V1189,
184 L1193, L1197 and I1198 (Fig. 2c). The hydrophobic interactions between HR1 and
185 HR2 are mainly located in the helical fusion core region, which will be discussed
186 later.

187 The overall 6-HB structure of SARS-CoV-2 is similar to that of other HCoVs
188 with root-mean-square deviation (RMSD) of 0.36 Å to SARS-CoV 6-HB and 0.66 Å
189 to MERS-CoV 6-HB for all the Cα atoms (Fig. 2d). This finding suggested that the
190 overall 6-HB conformation is an important and highly conserved component for these
191 dangerous coronaviruses. When comparing with the 6-HB of other common
192 coronaviruses causing mild respiratory disease, such as 229E and NL63, the
193 SARS-CoV-2 6-HB has a similar overall structure, except for the different length of
194 HR2 helix in the 6-HB. The HR2 domain of 229E or NL63 forms a longer and

bioRxiv preprint doi: https://doi.org/10.1101/2020.03.09.983247. this version posted March 12, 2020. The copyright holder for this preprint (which was not certified by peer review) is the author/funder. All rights reserved. No reuse allowed without permission.

195 bending helix to interact with trimeric HR1 core (Fig. 2e). The relationship between
196 the structural difference and the pathogenicity of these HCoVs remains to be
197 elucidated.

198 According to sequence alignment, the S2 subunits of SARS-CoV-2 and
199 SARS-CoV are highly conserved, with 92.6% and 100% overall homology in HR1
200 and HR2 domains, respectively. Inside the fusion core region of HR1 domain, there
201 are 8 different residues (Fig. 3a), which may contribute the enhanced interactions
202 between HR1 and HR2 and stabilize 6-HB conformation of SARS-CoV-2 as revealed
203 by crystallographic analysis, compared with those of SARS-CoV. This significant
204 difference has not been observed in other SARS-like viruses, such as WIV1, Rs3367,
205 and RsSHC014. As shown in Figure 3b, the K911 in SARS-CoV HR1 could bind to
206 E1176 in HR2 through a salt bridge 2.9 Å in distance. However, with the Lys-Ser
207 replacement, S929 in SARS-CoV-2 binds to S1196 through a strong hydrogen bond
208 2.4 Å in distance. In SARS-CoV, Q915 in the HR1 domain does not bind to the HR2
209 domain. However, with Q-K replacement in the new virus, K933 in the HR1 domain
210 binds to carbonyl oxygen of N1172 in HR2 through a salt bridge 2.7 Å in distance
211 (Fig. 3b). In SARS-CoV, E918 in the HR1 domain binds to R1166 in the HR2 domain
212 through a weak salt bridge 3.7 Å in distance. In SARS-CoV-2, E918 is mutated to
213 D936 and binds to R1185 in the HR2 domain through a salt bridge 2.7 Å in distance
214 (Fig. 3c). In SARS-CoV, K929 in HR1 binds to E1163 in HR2 through a salt bridge
215 3.2 Å in distance, while T925 is not involved in the interaction. However, when T925
216 was mutated to S943, it could bind to E1182 in the HR2 domain with a hydrogen
217 bond 2.6 Å in distance, and K947 could also bind to E1182 through a salt bridge 3.0
218 Å in distance (Fig. 3d). These results suggested that the multiple replacements in the
219 HR1 domain of emerging SARS-CoV-2 virus could enhance the interactions between
220 HR1 and HR2 domain to further stabilize the 6-HB structure, which may lead to
221 increased infectivity of the virus.

bioRxiv preprint doi: https://doi.org/10.1101/2020.03.09.983247. this version posted March 12, 2020. The copyright holder for this preprint (which was not certified by peer review) is the author/funder. All rights reserved. No reuse allowed without permission.

222 **Design and structure-activity relationship (SAR) analysis of lipopeptides with**
223 **remarkably improved fusion inhibitory activity**

224 Previously, we found that peptide EK1 could disturb viral 6-HB formation and
225 effectively inhibit SARS-CoV-2 PsV infection. However, the potent stability of
226 SARS-CoV-2 6-HB structure might reduce the antiviral efficacy of EK1. Recently,
227 numerous reports have shown that the lipidation strategy can effectively improve the
228 antiviral activity of fusion inhibitory peptides, such as the ant-HIV-1 peptide LP-19 [18],
229 and the anti-Nipah virus lipopeptides [19]. In order to improve the inhibitory activity of
230 EK1, cholesterol (Chol) and palmitic acid (Palm) were covalently attached to the
231 C-terminus of EK1 sequence under the help of a flexible polyethylene glycol (PEG)
232 spacer, and the corresponding lipopeptides EK1C and EK1P were constructed,
233 respectively (Fig. 4a). Both of them could completely inhibit SARS-CoV-2 mediated
234 cell-cell fusion at the concentration of 2.5 μM (Fig. 4b). The inhibitory activity with
235 mean 50% inhibitory concentration (IC_{50}) values is 48.1 nM for EK1C and 69.2 nM
236 for EK1P, respectively (Fig. 4c). Meanwhile, the EK1-scrambled peptide showed no
237 inhibitory activity with the concentration up to 5 μM (Fig. 4c). These results strongly
238 suggest that lipidation of EK1 is a promising strategy to improve its fusion-inhibitory
239 activity against SARS-CoV-2 infection, especially, cholesterol-modification.

240 On the basis of the structure of EK1C, series of cholesteryl EK1 with multiple
241 linkers were constructed, where the glycine/serine-based linker, *i.e.*, GSG, or
242 PEG-based spacer was employed between EK1 and the cholesterol moiety (Fig. 4d).
243 Compared with EK1C1, EK1C2 and EK1C showed similar inhibitory activities.
244 Strikingly, EK1C3 peptide with both the 3-amino acid linker "GSG" and the
245 PEG4-based spacer, exhibited 4-fold more potency than EK1C1. It is noteworthy that
246 changing "GSG" in EK1C3 to a longer 5-amino acid linker "GSGSG" significantly
247 increased the inhibitory potency of the hybrid molecule, and EK1C4 had IC_{50} value of
248 1.3 nM, which was 43-fold more potent than EK1C1. These findings indicate that the
249 linker length has a significant effect on the overall activity of lipopeptides.

bioRxiv preprint doi: https://doi.org/10.1101/2020.03.09.983247. this version posted March 12, 2020. The copyright holder for this preprint (which was not certified by peer review) is the author/funder. All rights reserved. No reuse allowed without permission.

250 Comparison of increasing PEG-based arm lengths in EK1C4 shows that inhibitors
251 potency slightly decreased in the cell-cell fusion assay (Fig. 4e). The data suggest that
252 "GSGSG-PEG4" linker was optimal to bridge both parts of the conjugates. Similarly,
253 EK1C4 showed the most potent inhibitory activity against SARS-CoV-2 PsV
254 infection, with IC_{50} value of 15.8 nM, providing 149-fold stronger anti-SARS-CoV-2
255 activity than that of EK1 (IC_{50}=2,375 nM) (Fig. 4f).

256 **The lipopeptide EK1C4 exhibits the most potent inhibitory activity against**
257 **membrane fusion mediated by S proteins and entry of pseudotyped**
258 **coronaviruses**

259 We have previously demonstrated that EK1 could effectively inhibit divergent
260 HCoV infection by targeting the HR1 domains, including α-HCoV and β-HCoV. Here,
261 we further systematically evaluated the broad-spectrum surface-fusion inhibitory
262 activity of EK1C4 on cell-cell fusion mediated by S proteins of divergent
263 coronaviruses, including SARS-CoV, MERS-CoV, HCoV-OC43, HCoV-NL63 and
264 HCoV-229E. Among them, SARS-CoV has the closest relatives to SARS-CoV-2, and
265 its S protein-mediated cell-cell fusion could be effectively inhibited by EK1C4 with
266 IC_{50} of 4.3 nM, which is about 94-fold more active than that of EK1 (IC_{50} = 409.3 nM)
267 (Fig. 5a). Similarly, EK1C4 showed extremely potent fusion-inhibitory activity on
268 MERS-S- and OC43-S-mediated cell-cell fusion with IC_{50} of 2.5 nM and 7.7 nM,
269 which were 95- and 101-fold more potent when compared to EK1, respectively,
270 indicating that EK1C4 could potently and broadly inhibit S protein-mediated cell-cell
271 fusion of various β-HCoVs (Fig. 5b-c). For α-HCoVs, EK1C4 also effectively
272 blocked the fusion process mediated by the S protein of HCoV-229E and
273 HCoV-NL63 with IC_{50} of 5.2 nM and 21.4 nM, respectively, while EK1 showed
274 inhibitory activity of IC_{50} ranging from 207.4 to 751.0 nM (Fig. 5d-e). Moreover, with
275 their potential for human infection, SL-CoVs, including WIV1, Rs3367 and
276 RsSHC014, the fusion process of which is mediated by S protein, could also be
277 significantly prevented by EK1C4 with IC_{50} ranging from 4.3 to 8.1 nM, as well as

bioRxiv preprint doi: https://doi.org/10.1101/2020.03.09.983247. this version posted March 12, 2020. The copyright holder for this preprint (which was not certified by peer review) is the author/funder. All rights reserved. No reuse allowed without permission.

278 EK with IC_{50} ranging from 237.0 to 279.6 nM (Fig. 5f-h). As control, the
279 EK1-scrambled peptide showed no inhibitory activity with concentration up to 5 μM
280 in all those coronavirus cell-cell fusion assays (Fig. 5a-h).

281 We also assessed the antiviral activity of EK1C4 on PsV infection by divergent
282 coronaviruses. As expected, EK1C4 showed much more potent activity than EK1
283 (IC_{50} ranging from 631.8 to 3237.0 nM) against SARS-CoV, MERS-CoV, and
284 HCoV-OC43 infection with IC_{50} of 11.7 nM, 11.1 nM and 37.7 nM, respectively (Fig.
285 5i-k). EK1C4 also effectively blocked PsV infection of α-HCoVs, including
286 HCoV-229E and HCoV-NL63, with IC_{50} of 12.4 nM and 76.6 nM, respectively,
287 which was about 319- and 99-fold more active than EK1 (IC_{50} ranging from 3,963 to
288 7,666 nM) (Fig. 5l-m). Similarly, by cholesteryl modification with "GSGSG-PEG4"
289 linker, the inhibitory activity of EK1 could be significantly increased on PsV infection
290 from SL-CoVs, including WIV1 and Rs3367, where EK1C4 showed potent inhibitory
291 activity with IC_{50} of 30.8 nM and 66.9 nM, respectively, which is 175-fold to 89-fold
292 more potent than that of EK1 (Fig. 5n-o).

293 **EK1C4 possesses the most potent inhibitory activity against *in vitro* infection by**
294 **live coronaviruses**

295 We further assessed the inhibitory activity of EK1C4 against live HCoVs infection,
296 including SARS-CoV-2, MERS-CoV, HCoV-OC43, HCoV-229E, and HCoV-NL63.
297 Importantly, EK1C4 effectively blocked SARS-CoV-2 infection at the cellular level
298 in a dose-dependent manner with IC_{50} of 36.5 nM, being 67-fold more active than that
299 of EK1 (IC_{50}=2,468 nM) (Fig. 6a), which is consistent to the results of cell-cell fusion
300 assay and PsV infection assay mediated by SARS-CoV-2 S protein. Similarly, EK1C4
301 also showed more potent antiviral activity than EK1 against MERS-CoV,
302 HCoV-OC43, HCoV-229E, and HCoV-NL63 infection with IC_{50}s of 4.2 nM, 24.8
303 nM, 101.5 nM and 187.6 nM, respectively, which are 190-, 62-, 42- and 19-fold more
304 potent than those of EK1, respectively (Fig. 6b-e). We next assessed the cytotoxicity
305 of EK1C4 on various target cells and found that the half cytotoxic concentration

bioRxiv preprint doi: https://doi.org/10.1101/2020.03.09.983247. this version posted March 12, 2020. The copyright holder for this preprint (which was not certified by peer review) is the author/funder. All rights reserved. No reuse allowed without permission.

306 (CC_{50}) was beyond 5 μM, which is the highest detection concentration of EK1C4 (Fig.
307 S3). Therefore, the selectivity index ($SI=CC_{50}/IC_{50}$) of EK1C4 is >136, suggesting
308 that EK1C4 is a promising SARS-CoV-2 fusion inhibitor with little, or even no, toxic
309 effect *in vitro*. Further, we explored the potent antiviral mechanism of EK1C4 and
310 found that the complexes of EK1C4/SARS-2HR1, EK1C4/MERS-HR1, and
311 EK1C4/SARS-2HR1 harbor higher stability and increased *Tm* values than those of the
312 complexes formed by EK1 and HR1s (Fig. S4). These results suggested that increased
313 antiviral activity of EK1C4 should be related its increased binding affinity with HR1,
314 but their detailed interactions require further studies.

315 **Intranasally applied EK1C4 showed strong protection of mice against**
316 **HCoV-OC43 infection**

317 Recently, SARS-CoV-2 rapidly spread in humans by transmitting through the
318 respiratory tract. Here, we used an HCoV-OC43 infection mouse model to further
319 investigate the potential prophylactic effect of EK1C4 in clinical applications *via* the
320 intranasal administration route (Fig. 6f-g). In the OC43-infected mouse model, we
321 treated newborn mice with EK1C4 at a single dose of 0.5 mg/kg 0.5 h (Pre-0.5), 2 h
322 (Pre-2), 4 h (Pre-4), 12 (Pre-12) and 24 h (Pre-24) before challenging with
323 HCoV-OC43 at 100 $TCID_{50}$ (50% tissue culture infectious dose). Starting from 4 days'
324 post-infection (dpi), the body weight of mice in the viral control group decreased
325 significantly along with 100% mortality (Fig. 6f-g). The final survival rates of mice in
326 Pre-0.5, Pre-2, Pre-4, Pre-12 and Pre-24 groups were 100%, 100%, 100%, 83% and
327 0%, respectively (Fig. 6f-g). In contrast, EK1 with a single dose of 20 mg/kg via nasal
328 administration exhibited very promising prophylactic effect in the Pre-0.5 h and Pre-1
329 h groups, whereas all mice in the EK1-Pre-2 h group eventually died similarly to the
330 mice in the viral control group (Fig. S5). These results suggested that EK1C4 has
331 better stability, antiviral activity, and prolonged half-life in the airway environment
332 when compared with EK1.

bioRxiv preprint doi: https://doi.org/10.1101/2020.03.09.983247. this version posted March 12, 2020. The copyright holder for this preprint (which was not certified by peer review) is the author/funder. All rights reserved. No reuse allowed without permission.

333 We then tested the therapeutic effect of EK1C4 0.5 h (Post-0.5 group) and 2 h
334 (Post-2 group) after HCoV-OC43 infection (Fig. 6h-i). The Post-0.5 group and Post-2
335 group mice showed 100% and 16.7% survival rate, respectively, suggesting that
336 EK1C4 harbors good therapeutic effect after a short period of HCoV-OC43 infection,
337 possibly resulting from the establishment of HCoV-OC43 infection in mouse brain
338 where EK1C4 cannot get through the blood brain barrier via nasal administration[14].
339 As shown in Fig. S6, high viral titer was detected in brains of all 5 mice in Pre-24
340 group and 4 out of 5 mice in Post-2 group, but was not detected in brain tissues of all
341 mice in Pre-0.5, Pre-2, Pre-4, and Post-0.5 groups, while only moderate level of viral
342 titer was detected in brain tissue in one of the 5 mice in Pre-12 group (Fig. S6 a and b).
343 Similar to those in the viral control mice, mice in Pre-24 and Post-2 groups exhibited
344 similar histopathological changes in brain tissues, including vacuolation, degeneration,
345 and infiltration. However, the brain tissues of mice in Pre-0.5, Pre-2, Pre-4, Pre-12
346 and Post-0.5 group as well as the normal control group showed no apparent
347 histopathological changes (Fig. S6 c).

348 **Discussion**

349 Over the past 20 years, highly infectious pathogens have been emerging
350 increasingly, such as SARS-CoV in 2003 and MERS-CoV in 2012 [20-22]. In 2018,
351 WHO proposed "Disease X" in the blueprint priority diseases for any new unknown
352 pathogen that may cause an epidemic or pandemic in the future, calling for the
353 development of effective and safe vaccines and antivirals to prevent and treat such
354 Disease X. Indeed, at the end of 2019, the outbreak of Wuhan pneumonia with an
355 unknown etiological agent, the first Disease X following WHO's announcement was
356 reported to WHO. Shortly thereafter, a novel coronavirus, SARS-CoV-2 (also known
357 as 2019-nCoV or HCoV-19), was identified to be the etiology of the Wuhan
358 pneumonia, *i.e.,* COVID-19 as designated by WHO.

359 Unlike SARS-CoV, live SARS-CoV-2-infected cells were found to form typical
360 syncytium, suggesting that SARS-CoV-2 may mainly utilize the plasma membrane

bioRxiv preprint doi: https://doi.org/10.1101/2020.03.09.983247. this version posted March 12, 2020. The copyright holder for this preprint (which was not certified by peer review) is the author/funder. All rights reserved. No reuse allowed without permission.

361 fusion pathway to enter and replicate inside host cells. Consistently, in the cell-cell
362 fusion system, SARS-CoV-2 S protein could effectively mediate the formation of
363 syncytium between the effector cell and the target cell in the absence of an exogenous
364 proteolytic enzyme, e.g., trypsin, while SARS-CoV S protein could not. Actually, the
365 plasma membrane fusion pathway is more efficient than the endosomal membrane
366 fusion pathway for most viruses because the latter is more prone to activating the host
367 cell antiviral immunity[23,24]. Generally, β-B coronaviruses lack the S1/S2
368 furin-recognition site, and their S proteins are uncleaved in the native state. For
369 example, SARS-CoV enters into the cell mainly *via* the endosomal membrane fusion
370 pathway where its S protein is cleaved by endosomal cathepsin L and activated[25].
371 Inducing the S1/S2 furin-recognition site could significantly increase the capacity of
372 SARS-CoV S protein to mediate cellular membrane surface infection [26]. Interestingly,
373 SARS-CoV-2 harbors the S1/S2 cleavage site in its S protein, but its specific role in S
374 protein-mediated membrane fusion and viral life-cycle remains to be further explored
375 (Fig. S7). A recent report suggested that SARS-CoV-2 mainly used TMPRSS2 for
376 plasma membrane fusion; this means that the TMPRSS2 inhibitor might constitute an
377 option for blocking SARS-CoV-2 fusion with and entry into the host cell [27].

378 The 6-HB structure formed by HR1 and HR2 regions in the S2 subunit of HCoVs
379 plays a key role during the viral membrane fusion process, which makes it one of the
380 most important targets for drug design. In previous studies, we have found that HR1
381 and HR2 of SARS-CoV-2 could form a stable coiled-coil complex, but the detailed
382 conformations remain unknown. According to the X-ray crystallographic analysis of
383 the complex formed by HR1 and HR2 of SARS-CoV-2 (Fig. 2b), it is a typical 6-HB
384 fusion core structure similar to those of SARS-CoV and MERS-CoV. Although the
385 amino acid sequences of HR2 domain from SARS-CoV and SARS-CoV-2 are fully
386 identical, multiple residue differences occur in the HR1 domain of SARS-CoV-2.
387 However, instead of weakening the interaction between HR1 and HR2, such unilateral
388 difference seems to form new interactions in some regions and enhance the existing
389 ones in other regions (Fig. 3). When K991 in SARS-CoV HR1 was replaced with

bioRxiv preprint doi: https://doi.org/10.1101/2020.03.09.983247. this version posted March 12, 2020. The copyright holder for this preprint (which was not certified by peer review) is the author/funder. All rights reserved. No reuse allowed without permission.

390 S929 in SARS-CoV2 HR1, a new, strong hydrogen bond was formed with a distance
391 of 2.4 Å. K933 forms a new interaction with N1192 in SARS-CoV-2 with a distance
392 of 2.7 Å, whereas the corresponding position in SARS-CoV has no such interaction.
393 In the other two regions, E918 binds to R1166 and K929 binds to E1163 in
394 SARS-CoV, both of which were enhanced in SARS-CoV-2. These results suggest that
395 this new HCoV has evolved with improved binding affinity between HR1 and HR2
396 domains, which may accelerate the viral membrane fusion process and enhance viral
397 infectivity or transmissibility. A recent study also found that the binding affinity
398 between ACE2 receptor on the host cell and RBD in S protein of SARS-CoV-2 is
399 more than 10-fold higher than that of SARS-CoV, which may also be associated with
400 the increased infectivity and transmissibility of SARS-CoV-2[12].

401 The conjugation of cholesterol to viral entry inhibitor has been proved to be an
402 effective strategy to enhance the antiviral activity, such as C34 peptide for HIV-1 [28].
403 However, the mechanism of this enhancement, especially the role of cholesterol group
404 in the C-terminal tail of entry inhibitor, is still unclear. There is a possibility that the
405 cholesterol group could anchor to the target membrane to facilitate the binding of
406 inhibitor to the HR1 targets. However, we noticed that binding affinity between
407 EK1C4 and SARS-CoV-2-HR1P is significantly enhanced than EK1 peptide alone,
408 which suggested that cholesterol group may be involved in binding to HR1P directly
409 (Fig. S4). Therefore, using structural simulation and docking method, we predicted a
410 possible model of EK1C4 in binding with SARS-CoV-2 HR1P (Fig. S8). In this
411 model, the EK1C4 peptide anchors to one of the three hydrophobic grooves of HR1
412 trimer via its EK1 moiety, and also anchors to another adjacent hydrophobic groove of
413 HR1 trimer via its cholesterol moiety. The cholesterol group of EK1C4 may bind to
414 HR1P through hydrophobic interactions, while several hydrogen bonds may form
415 between HR1 and helical region of EK1C4. The intermediated GSGSG-PEG4 linker
416 of EK1C4 peptide is just enough to connect these two moieties on the two binding
417 targets. Admittedly, the exact mechanism and structure of EK1C4 need more studies
418 in the future.

bioRxiv preprint doi: https://doi.org/10.1101/2020.03.09.983247. this version posted March 12, 2020. The copyright holder for this preprint (which was not certified by peer review) is the author/funder. All rights reserved. No reuse allowed without permission.

419 In the past few decades, the viral HR1 domain has been proved to be an important
420 target for the development of viral fusion and entry inhibitors. In the early outbreak of
421 MERS, we quickly solved the 6-HB fusion core structure formed by MERS-CoV S
422 protein HR1 and HR2 domains and designed the fusion inhibitory peptide HR2P-M2
423 which proved to be highly effective in blocking its spike protein-mediated membrane
424 fusion and inhibit *in vitro* MERS-CoV infection[16]. The results from animal
425 experiments showed that intranasal application of HR2P-M2 peptide could effectively
426 protect mice from MERS-CoV infection with reduction of virus titers in the lung
427 more than 1000-fold[29]. However, the MERS-CoV HR2P-M2 peptide could not inhibit
428 SARS-CoV infection, suggesting that this peptide lacks cross-inhibitory activity
429 against other β-CoVs, such as SARS-CoV and bat SARSr-CoVs. To be well prepared
430 for combating the emerging coronaviruses with epidemic or pandemic potential, we
431 designed and synthesized the first pan-coronavirus fusion inhibitor, EK1, and found
432 that EK1 exhibited potent inhibitory activity against all HCoVs that we tested,
433 including SARS-CoV and MARS-CoV, as well as bat SARSr-CoVs. As expected, we
434 recently have shown that EK1 is also effective in inhibiting infection of the novel
435 β-CoV, SARS-CoV-2 [15]. We then optimized EK1 peptide in hopes of improving its
436 fusion inhibitory activity. Indeed, we found that one of the modified EK1 peptides,
437 EK1C4, was 226-fold and 149-fold more potent against SARS-CoV-2 S
438 protein-mediated membrane fusion and PsV infection, respectively, than EK1. EK1C4
439 also showed broad-spectrum inhibitory activity against infection by SARS-CoV,
440 MERS-CoV and other HCoVs. EK1C4 showed prolonged and significant
441 prophylactic effect against HCoV-OC43 infection in mouse model, suggesting that
442 EK1C4 may also be used as an inhibitor against SARS-CoV-2 infection *in vivo*.
443 Consistent with other studies [35], HCoV-OC43 was showed as a typical neurotropic
444 virus in the mouse model, and quickly entered and established infection in mouse
445 brain tissue, leading to the relatively weak therapeutic effect of EK1C4 via intranasal
446 administration. However, SARS-CoV-2 mainly infected and caused severe
447 pathological changes in human lung tissue [4]. Therefore, EK1C4 administered

bioRxiv preprint doi: https://doi.org/10.1101/2020.03.09.983247. this version posted March 12, 2020. The copyright holder for this preprint (which was not certified by peer review) is the author/funder. All rights reserved. No reuse allowed without permission.

448 intranasally is expected to have good therapeutic potential against SARS-CoV-2
449 infection.

450 Currently, no specific anti-CoV therapeutics or prophylactics have been used in
451 clinics for treatment or prevention of SARS-CoV-2 infection. A number of
452 nonspecific antiviral drugs, including IFN, lopinavir-ritonavir (HIV protease
453 inhibitors), chloroquine, favipiravir (T-705) and remdesivir (GS-5734), have been
454 used in clinics in China to treat SARS-CoV-2 infection [30]. Their *in vivo* efficacies still
455 require further confirmation. Their potential use for treatment of infection by other
456 coronaviruses and emerging coronaviruses in the future is unclear. Compared with
457 these clinically used nonspecific antiviral drugs, EK1C4 has more advantages for
458 treatment and prevention of SARS-CoV-2 infection. First, the sequence of its target,
459 the HR1 domain in S2 subunit of S protein, is highly conserved. Therefore, EK1C4
460 possesses a high genetic barrier to resistance and cannot easily induce drug-resistant
461 mutations. Second, EK1C4 can be used in an intranasal formulation to prevent
462 coronavirus infection. The small bottles can be carried easily by persons who will
463 have close contact with infected patients or high-risk populations. Third, EK1C4 can
464 be used in inhalation formulation for treatment of patients to reduce the viral loads in
465 their lungs, thus attenuating the acute lung injury caused by viral infection and
466 reducing the chance to spread the virions to the closely contacted persons. The
467 inhalation equipment can be used in home or hotel room, reducing the expense of
468 staying in hospitals. Fourth, EK1C4 is expected to be safe to humans because it will
469 be used locally, not systemically, and peptide drugs are generally safer than chemical
470 drugs. Fifth, because of its broad-spectrum anti-coronavirus activity, EK1C4 can be
471 used for treatment and prevention of infection by not only SARS-CoV-2, but also
472 other HCoVs. Sixth, recently 103 SARS-CoV-2 genomes have been identified [31], but
473 we found that both the HR1 and HR2 domains among those reported genomes show
474 100% identity (Fig. S9), indicating the high conservation of EK1C4 target. In the
475 meantime, the HR2 derived peptides have much larger interface on HR1 domain,
476 making it more resistant to the viral mutations. Therefore, EK1C4 shows exceptional

bioRxiv preprint doi: https://doi.org/10.1101/2020.03.09.983247. this version posted March 12, 2020. The copyright holder for this preprint (which was not certified by peer review) is the author/funder. All rights reserved. No reuse allowed without permission.

477 promise to be developed as the first pan-CoV fusion inhibitor-based antiviral
478 therapeutic or prophylactic for treatment or prevention of infection by the currently
479 circulating SARS-CoV-2 and MERS-CoV and the future reemerging SARS-CoV and
480 emerging SARSr-CoVs.

481 **Methods**

482 Cell Lines, viruses and Peptides

483 The human primary embryonic kidney cell line (293T) (CRL-3216™), Calu-3
484 (HTB-55™), A549 (CCL-185), Vero E6 (CRL-1586™), RD (CCL-136™), and
485 LLC-MK2 Original (CCL-7™) cells were obtained from the American Type Culture
486 Collection (ATCC). Human hepatoma Huh-7 cells were from the Cell Bank of the
487 Chinese Academy of Sciences (Shanghai, China), and 293T cells stably expressing
488 human ACE2 (293T/ACE2) cells were kindly provided by Dr. Lanying Du. All of
489 these cell lines were maintained and grown in Dulbecco's Modified Eagle's Medium
490 (DMEM, Invitrogen, Carlsbad, CA, USA) containing 100 U/ml penicillin, 100 mg/ml
491 streptomycin, and 10% heat-inactivated fetal calf serum (FCS) (Gibco).

492 Patient-derived COVID-19 (BetaCoV/Wuhan/WIV04/2019) was isolated by the
493 Wuhan Institute of Virology [6]. MERS-CoV-EMC/2012 was originally provided by
494 Chuan Qin (Beijing Key Laboratory for Animal Models of Emerging and
495 Re-emerging Infectious Diseases). ATCC strain of Human coronavirus 229E
496 (HCoV-OC43, VR-740), as well as Human coronavirus OC43 (HCoV-229E, VR-1558)
497 and HCoV-NL63 (Amsterdam strain) strains were amplified in Huh-7, HCT-8 and
498 LLC-MK2 cells, respectively.

499 Peptides were synthesized by Chao Wang (Beijing Institute of Pharmacology and
500 Toxicology). The sequences of EK1
501 (SLDQINVTFLDLEYEMKKLEEAIKKLEESYIDLKEL) and EK1-scrambled
502 (LKVLLYEEFKLLESLIMEILEYQKDSDIKENAEDTK) have been reported in our
503 previous study [14]

bioRxiv preprint doi: https://doi.org/10.1101/2020.03.09.983247. this version posted March 12, 2020. The copyright holder for this preprint (which was not certified by peer review) is the author/funder. All rights reserved. No reuse allowed without permission.

504

505 **Plasmids**

506 The envelope-expressing plasmids of SARS-2-S (pcDNA3.1-SARS-2-S), SARS-S
507 (pcDNA3.1-SARS-S), MERS-S (pcDNA3.1-MERS-S), OC43-S
508 (pcDNA3.1-OC43-S), NL63-S (pcDNA3.1-NL63-S), 229E-S (pcDNA3.1-229E-S),
509 and bat SARS-like CoV-S (pcDNA3.1-WIV1-S, pcDNA3.1-Rs3367-S and
510 pcDNA3.1-SHC014-S), and the plasmids pAAV-IRES-EGFP that encode EGFP as
511 well as the luciferase reporter vector (pNL4-3.Luc.R-E-) were maintained in our
512 laboratory.

513 **Cell–cell fusion assay**

514 The establishment and detection of several cell–cell fusion assays are as previously
515 described [14,16]. In brief, Huh-7 cells (for testing all coronaviruses) or 293T/ACE2 cells
516 (for testing SARS-CoV-2) were used as target cells. For preparing effector cells
517 expressing S protein a coronavirus, 293T cells were transfected with one of the S
518 protein expression vectors, including 293T/SARS-CoV-2/GFP,
519 293T/MERS-CoV/GFP, 293T/HCoV-229E/GFP, 293T/SARS-CoV/GFP, or
520 293T/SL-CoV/GFP, 293T/HCoV-OC43/GFP, 293T/HCoV-NL63/GFP or empty
521 plasmid pAAV-IRES-EGFP. For SARS-CoV S-, SL-CoV S-, OC43 S- or NL63
522 S-mediated cell-cell fusion assays, effector cells and target cells were cocultured in
523 DMEM containing trypsin (80 ng/mL) for 4 h, while for SARS-CoV-2 and
524 MERS-CoV S-mediated cell-cell fusion assays, effector cells and target cells were
525 cocultured in DMEM without trypsin but 10% FBS for 2 h. After incubation, five
526 fields were randomly selected in each well to count the number of fused and unfused
527 cells under an inverted fluorescence microscope (Nikon Eclipse Ti-S).

528 **Inhibition of HCoV S-mediated cell-cell fusion**

529 The inhibitory activity of a peptide on a HCoV S-mediated cell-cell fusion was
530 assessed as previously described[14,16]. Briefly, a total of 2×10^4 cells/well target cells

bioRxiv preprint doi: https://doi.org/10.1101/2020.03.09.983247. this version posted March 12, 2020. The copyright holder for this preprint (which was not certified by peer review) is the author/funder. All rights reserved. No reuse allowed without permission.

531 (Huh-7) were incubated for 5 h. Afterwards, 10^4 cells/well effector cells (293T/S/GFP)
532 were added in the presence or absence of a peptide at the indicated concentrations at
533 37 °C for 2 h. 293T/EGFP cells with phosphate-buffered saline (PBS) were used as a
534 negative control. The fusion rate was calculated by observing the fused and unfused
535 cells using fluorescence microscopy.

536 **Inhibition of pseudotyped HCoV infection**

537 293T cells were cotransfected with pNL4-3.luc.RE (the luciferase reporter-expressing
538 HIV-1 backbone) and pcDNA3.1-SARS-CoV-2-S (encoding for CoVs S protein)
539 using VigoFect (Vigorous Biotechnology, Beijing, China) [16,32,33]. Pseudotyped
540 particles were efficiently released in the supernatant. The supernatant was harvested at
541 72 h post-transfection, centrifuged at 3000× g for 10 min, and frozen to −80 °C. To
542 detect the inhibitory activity of a peptide on infection of coronavirus PsV, target cells
543 (293T/ACE2 for SARS-CoV-2, SARS-CoV and SL-CoVs; RD cells for HCoV-OC43;
544 Huh-7 for other CoVs) were plated at a density of 10^4 cells per well in a 96-well plate
545 one day prior to infection [14]. PsV was mixed with an equal volume of a peptide which
546 was series diluted with PBS at 37 °C for 30 min. The mixture was transferred to the
547 Huh-7 cells. Medium was changed after 12 h and incubation continued for 48 h.
548 Luciferase activity was analyzed by the Luciferase Assay System (Promega, Madison,
549 WI, USA).

550 **Inhibition of live HCoV replication**

551 The inhibition assay for live SARS-CoV-2 and MERS-CoV was performed in a
552 biosafety level 3 (BSL3) facility at the Wuhan Research Institute and Beijing Key
553 Laboratory for Animal Models of Emerging and Re-emerging Infectious Diseases,
554 respectively[6]. Inhibition activity of peptides on SARS-CoV-2 and MERS-CoV was
555 determined by plaque reduction assay. Peptides with different dilution concentrations
556 were mixed with SARS-CoV-2 (100 TCID50) for 30 minutes and then added to
557 monolayer VERO-E6 cells. After adsorption at 37 °C, the supernatant was removed,
558 and 0.9 % methyl cellulose was overlaid on the cells. After 72 h, the plates were fixed

bioRxiv preprint doi: https://doi.org/10.1101/2020.03.09.983247. this version posted March 12, 2020. The copyright holder for this preprint (which was not certified by peer review) is the author/funder. All rights reserved. No reuse allowed without permission.

559 and stained. Plaques were counted by fixing with 4% paraformaldehyde and staining
560 with 0.1% crystal violet. To test the effect of peptide on HCoV-OC43, HCoV-229E
561 and HCoV-NL63 replication, 50 μL of 100 TCID50 virus were mixed with an equal
562 volume of peptide and incubated at 37 ° C for 1 hour. Afterwards, the mixture was
563 added to RD, Huh-7 and LLC-MK2 cells, respectively. Cell Counting Kit-8 (CCK8,
564 Dojindo, Kumamoto, Kyushu, Japan) assay was applied to determine cytopathic
565 effect.

566 **Circular dichroism spectroscopy**

567 The peptides or peptide mixtures were dissolved in PBS to prepare a solution with a
568 final concentration of 10 μM at 37 °C for 30 min and then measured on a Jasco-815-
569 circular dichroism spectrometer [34]. The scanning wavelength range was 198-260 nm.
570 Thermal denaturation detection starts at 222 nm with a 5 °C/min thermal gradient
571 detection.

572 **Mouse infection studies**

573 Newborn mice were bred from pregnant mice purchased from the Animal Center of
574 Fudan University, and all the related experiments were carried out in strict accordance
575 with institutional regulations (approval number 20190221-070, approval date 21
576 February 2019). Each group had 12 3-day-old mice. To test the protective effect of
577 peptides on HCoV-infected mice, EK1C4 (0.5 mg/kg), EK1 (20 mg/kg) in 2 μl 28%
578 Hydroxypropyl-β-Cyclodextrin (HBC), or phosphate-buffered saline (PBS) solution,
579 were administered intranasally 0.5, 1, 2, 4, 12, and 24 h before challenge, or 0.5 and 2
580 h after challenge . Then mice were challenged intranasally with HCoV at a dose of
581 10^2 TCID50. For the viral control group, the same volume of 28% HBC or PBS was
582 administered intranasally. In each group, six mice were randomly selected for
583 euthanasia on day 5 after infection, then five mice for collecting and assessing the
584 viral titer in mouse brain, one mouse for brain histological examination. Body weight
585 and survival of the remaining six mice in each group were monitored for 14 days [35]

bioRxiv preprint doi: https://doi.org/10.1101/2020.03.09.983247. this version posted March 12, 2020. The copyright holder for this preprint (which was not certified by peer review) is the author/funder. All rights reserved. No reuse allowed without permission.

586 **Cytotoxicity assay**

587 Cytotoxicity of the peptides to the cells (Vero-E6, Huh-7, LLC-MK2 and RD cells)
588 was tested by using the Cell Counting Kit-8 (CCK-8). Briefly, each cell type was
589 seeded into the wells of a 96-well microtiter plate (10,000 per well) and incubated at
590 37 °C for 12-15 h, replacing medium with DMED containing EK1C4 at graded
591 concentrations to culture at 37 °C for 2 days; CCK-8 solution (10 μL per well) was
592 added, followed by an additional incubation for 4 h. The absorbance was measured at
593 450 nm.

594 **Expression and purification of fusion protein HR1-L6-HR2 of SARS-CoV-2**

595 The coding sequences of HR1 (residues 910 to 988) and HR2 (residues 1162 to 1206)
596 domains of SARS-CoV-2 S2 subunits were tandem linked though a 6-residue linker
597 (L6: SGGRGG). The resulting sequences encoding the fused HR1-L6-HR2 protein
598 were then cloned into a modified pET-28a vector containing a His_6-SUMO tag
599 upstream of the multiple cloning site. The recombinant construct was expressed in
600 *Escherichia coli* BL21 (DE3). Cells were grown in lysogeny broth (LB) media
601 supplemented with 50 μg/mL kanamycin at 37 °C and were induced with 1 mM IPTG
602 for 12 h at 16 °C overnight. Cells were harvested by centrifugation at 4500 g for 10
603 min at 4 °C and were lysed by high-pressure homogenizer twice after resuspension in
604 buffer containing 25 mM Tris–HCl, pH 8.0, and 200 mM NaCl. The fusion proteins
605 were isolated by Ni-affinity chromatography, and the SUMO tag was removed by
606 Ulp1 enzyme (1:100 w/w) cleavage. HR1-L6-HR2 protein was concentrated and
607 gel-filtered on a 10/300 Superdex 75 (GE Healthcare) column. Peak fractions
608 containing HR1-L6-HR2 trimer were pooled and concentrated to 20 mg/ml through
609 centrifugation (EMD Millipore).

610 **Crystallization and structure determination**

611 Crystals were obtained at 16 °C for 7 days using the hanging drop vapor diffusion
612 method by mixing equal volume of protein solution (HR1-L6-HR2, 10 mg/mL) and

bioRxiv preprint doi: https://doi.org/10.1101/2020.03.09.983247. this version posted March 12, 2020. The copyright holder for this preprint (which was not certified by peer review) is the author/funder. All rights reserved. No reuse allowed without permission.

613 reservoir solution (10% PEG8000, 200 mM zinc acetate, 0.1 M MES, pH 6.0). Then
614 crystals were flash-frozen and transferred to liquid nitrogen for data collection. On the
615 in-house (Institute of Biophysics, Chinese Academy of Sciences) X-ray source
616 (MicroMax 007 generator (Rigaku, Japan)) combined with Varimax HR optics
617 (Rigaku, Japan), HR1-L6-HR2 crystals at 100 K were diffracted to 2.9-Å resolution at
618 a wavelength of 1.5418 Å. A native set of X-ray diffraction data was collected with
619 the R-AXIS IV ++ detector (Rigaku, Japan) with an exposure time of 3 min per image
620 and was indexed and processed using iMosflm [36]. The space group of the collected
621 dataset is P21. Molecular replacement was performed with PHENIX.phaser [37] to solve
622 the phasing problem, using the SARS-CoV S protein core structure (PDB code
623 1WYY) as a search model. The final model was manually adjusted in COOT and
624 refined with Refmac [38]. Data collection statistics and refinement statistics are given in
625 Table 1. Coordinates were deposited in the RCSB Protein Data Bank (PDB code:
626 6LXT). The interaction model of EK1C4 peptide and HR1 domains of SARS-nCoV-2
627 was predicted by SWISS-MODEL sever [39] using 6XLT as reference for EK1 moiety,
628 and by Autodock 4 software [40] for cholesterol moiety (Fig. S8).

629 **Statistical analysis**

630 The survival rates of mice were analyzed by GraphPad Prism 5.0 software. CalcuSyn
631 software was kindly provided by T.C. Chou, and the percent inhibition and IC_{50}
632 values were calculated based on it [34].

633

634 **Conflicts of interest**

635 The authors declare no conflict of interest.

636

637

638 **References**

bioRxiv preprint doi: https://doi.org/10.1101/2020.03.09.983247. this version posted March 12, 2020. The copyright holder for this preprint (which was not certified by peer review) is the author/funder. All rights reserved. No reuse allowed without permission.

639 1. WHO. Blueprint for R&D preparedness and response to public health emergencies due to
640 highly infectious pathogens.
641 http://www.who.int/medicines/ebola-treatment/WHO-list-of-top-emerging-diseases/en/
642 (10 December 2015).
643 2. WHO. Prioritizing diseases for research and development in emergency contexts.
644 https://www.who.int/activities/prioritizing-diseases-for-research-and-development-in-eme
645 rgency-contexts (2019).
646 3. WHO. Coronavirus disease.
647 https://www.who.int/emergencies/diseases/novel-coronavirus-2019 (accessed Feb 23,
648 2020).
649 4. Zhu, N., *et al.* A novel Coronavirus from patients with pneumonia in China, 2019. *N. Engl.*
650 *J. Med.* 382, 727-733. (2020).
651 5. Wu, F., *et al.* A new coronavirus associated with human respiratory disease in China.
652 *Nature* https://doi.org/10.1038/s41586-020-2008-3 (2020).
653 6. Zhou, P., *et al.* A pneumonia outbreak associated with a new coronavirus of probable bat
654 origin. *Nature* doi: 10.1038/s41586-020-2012-7 (2020).
655 7. Gorbalenya, A., *et al.* Severe acute respiratory syndrome-related coronavirus: The species
656 and its viruses – a statement of the Coronavirus Study Group. Preprint at
657 https://doi.org/10.1101/2020.02.07.937862 (2020).
658 8. Jiang, S., Du, L. & Shi, Z. An emerging coronavirus causing pneumonia outbreak in
659 Wuhan, China: calling for developing therapeutic and prophylactic strategies. *Emerg.*
660 *Microbes. Infect.* **9**, 275-277 (2020).
661 9. Huang, C., *et al.* Clinical features of patients infected with 2019 novel coronavirus in
662 Wuhan, China. *Lancet* **395**, 497-506 (2020).
663 10. Jiang, S., *et al.* A distinct name is needed for the new coronavirus. *lancet*
664 https://doi.org/10.1016/S0140-6736(20)30419-0 (2020).
665 11. WHO. Coronavirus disease 2019 (COVID-19) Situation Report -32.
666 https://www.who.int/docs/default-source/coronaviruse/situation-reports/20200221-sitrep-
667 32-covid-19.pdf?sfvrsn=4802d089_2 (accessed Feb 21, 2020).
668 12. Wrapp, D., *et al.* Cryo-EM structure of the 2019-nCoV spike in the prefusion
669 conformation. https://doi.org/10.1101/2020.02.11.944462 (2020).
670 13. Bosch, B.J., *et al.* Severe acute respiratory syndrome coronavirus (SARS-CoV) infection
671 inhibition using spike protein heptad repeat-derived peptides. *Proc. Natl. Acad. Sci. U. S.*
672 *A.* **101**, 8455-8460 (2004).
673 14. Xia, S., *et al.* A pan-coronavirus fusion inhibitor targeting the HR1 domain of human
674 coronavirus spike. *Sci. Adv.* **5**, eaav4580 (2019).
675 15. Xia, S., *et al.* Fusion mechanism of 2019-nCoV and fusion inhibitors targeting HR1
676 domain in spike protein. *Cell Mol. Immunol.* doi: 10.1038/s41423-020-0374-2 (2020).
677 16. Lu, L., *et al.* Structure-based discovery of Middle East respiratory syndrome coronavirus
678 fusion inhibitor. *Nat. Commun.* **5**, 3067 (2014).
679 17. Liu, S., *et al.* Interaction between heptad repeat 1 and 2 regions in spike protein of
680 SARS-associated coronavirus: implications for virus fusogenic mechanism and
681 identification of fusion inhibitors. *Lancet* **363**, 938-947 (2004).
682 18. Chong, H., *et al.* A lipopeptide HIV-1/2 fusion inhibitor with highly potent in vitro, ex

bioRxiv preprint doi: https://doi.org/10.1101/2020.03.09.983247. this version posted March 12, 2020. The copyright holder for this preprint (which was not certified by peer review) is the author/funder. All rights reserved. No reuse allowed without permission.

683 vivo, and in vivo antiviral activity. *J. Virol.* **91**(2017).
684 19. Mathieu, C., *et al.* Fusion inhibitory lipopeptides engineered for prophylaxis of Nipah
685 virus in primates. *J. Infect. Dis.* **218**, 218-227 (2018).
686 20. Garten, R.J., *et al.* Antigenic and genetic characteristics of swine-origin 2009 A(H1N1)
687 influenza viruses circulating in humans. *Science* **325**, 197-201 (2009).
688 21. Anderson, L.J. & Baric, R.S. Emerging human coronaviruses--disease potential and
689 preparedness. *N. Engl. J. Med.* **367**, 1850-1852 (2012).
690 22. Howard, C.R. & Fletcher, N.F. Emerging virus diseases: can we ever expect the
691 unexpected? *Emerg. Microbes. Infect.* **1**, e46 (2012).
692 23. Shirato, K., Kanou, K., Kawase, M. & Matsuyama, S. Clinical isolates of human
693 coronavirus 229E bypass the endosome for cell entry. *J Virol* **91**(2017).
694 24. Shirato, K., Kawase, M. & Matsuyama, S. Wild-type human coronaviruses prefer
695 cell-surface TMPRSS2 to endosomal cathepsins for cell entry. *Virology* **517**, 9-15 (2018).
696 25. Belouzard, S., Chu, V.C. & Whittaker, G.R. Activation of the SARS coronavirus spike
697 protein via sequential proteolytic cleavage at two distinct sites. *Proc. Natl. Acad. Sci. U. S.*
698 *A.* **106**, 5871-5876 (2009).
699 26. Follis, K.E., York, J. & Nunberg, J.H. Furin cleavage of the SARS coronavirus spike
700 glycoprotein enhances cell-cell fusion but does not affect virion entry. *Virology* **350**,
701 358-369 (2006).
702 27. Hoffmann, M., *et al.* The novel coronavirus 2019 (2019-nCoV) uses the
703 SARS-coronavirus receptor ACE2 and the cellular protease TMPRSS2 for entry into
704 target cells. Preprint at https://doi.org/10.1101/2020.01.31.929042 (2020).
705 28. Hollmann, A., *et al.* Conjugation of cholesterol to HIV-1 fusion inhibitor C34 increases
706 peptide-membrane interactions potentiating its action. *PLoS One* **8**, e60302 (2013).
707 29. Channappanavar, R., *et al.* Protective effect of intranasal regimens containing peptidic
708 Middle East Respiratory Syndrome coronavirus fusion inhibitor against MERS-CoV
709 infection. *J. Infect. Dis.* **212**, 1894-1903 (2015).
710 30. Wang, M., *et al.* Remdesivir and chloroquine effectively inhibit the recently emerged
711 novel coronavirus (2019-nCoV) in vitro. *Cell Res* (2020). doi:
712 10.1038/s41422-020-0282-0. (2020)
713 31. Tang, X.L., *et al.* On the origin and continuing evolution of SARS-CoV-2. *Natl. Sci. Rev.*
714 (2020). Preprint at https://doi.org/10.1093/nsr/nwaa033 (2020)
715 32. Xia, S., *et al.* Potent MERS-CoV fusion inhibitory peptides identified from HR2 domain
716 in spike protein of bat coronavirus HKU4. *Viruses* **11**(2019).
717 33. Xia, S., *et al.* Peptide-Based membrane fusion inhibitors targeting HCoV-229E spike
718 protein HR1 and HR2 domains. *Int. J. Mol. Sci.* **19**(2018).
719 34. Chen, Y.H., et al. Determination of the helix and beta form of proteins in aqueous solution
720 676 by circular dichroism. Biochemistry, 13, 3350–3359 (1974)
721 35. Jacomy, H. & Talbot, P.J. Vacuolating encephalitis in mice infected by human coronavirus
722 OC43. *Virology* **315**, 20-33 (2003).
723 36. Battye, T.G., *et al.* iMOSFLM: a new graphical interface for diffraction-image processing
724 with MOSFLM. *Acta Crystallogr. D. Biol. Crystallogr.* **67**, 271-281 (2011).
725 37. Liebschner, D., *et al.* Macromolecular structure determination using X-rays, neutrons and
726 electrons: recent developments in Phenix. *Acta Crystallogr. D. Struct. Biol.* **75**, 861-877

bioRxiv preprint doi: https://doi.org/10.1101/2020.03.09.983247. this version posted March 12, 2020. The copyright holder for this preprint (which was not certified by peer review) is the author/funder. All rights reserved. No reuse allowed without permission.

727 (2019).
728 38. Vagin, A.A., *et al.* REFMAC5 dictionary: organization of prior chemical knowledge and
729 guidelines for its use. *Acta Crystallogr. D. Biol. Crystallogr.* **60**, 2184-2195 (2004).
730 39. Waterhouse, A., *et al.* SWISS-MODEL: homology modelling of protein structures and
731 complexes. *Nucleic Acids Res* **46**, W296-W303 (2018).
732 40. Morris, G.M., *et al.* AutoDock4 and AutoDockTools4: Automated docking with selective
733 receptor flexibility. *J Comput Chem* **30**, 2785-2791 (2009).
734

735

bioRxiv preprint doi: https://doi.org/10.1101/2020.03.09.983247. this version posted March 12, 2020. The copyright holder for this preprint (which was not certified by peer review) is the author/funder. All rights reserved. No reuse allowed without permission.

736 **Figure Legends**

737 **Fig. 1. Establishment of SARS-CoV-2 S protein-mediated cell-cell fusion system**

738 **a**. The emerging timeline for highly pathogenic viruses and the proposed Disease X. **b**.
739 Schematic representation of SARS-CoV-2 S protein. Its S1 subunit contains NTD
740 (14-305 aa), RBD (319-541 aa), and RBM (437-508 aa). Its S2 subunit contains FP
741 (788-806 aa), HR1 (912-984 aa), HR2 (1163-1213 aa), TM (1214-1237 aa) and CP
742 (1238-1273 aa). **c**. The formation of syncytium in Huh-7 cells 24 h after SARS-CoV-2
743 infection, with scale bar of 200 μm. **d**. Images of SARS-CoV- and SARS-CoV-2
744 S-mediated cell–cell fusion on 293T/ACE2 cells at 2 h (left) and 24 h (right). **e**.
745 SARS-CoV (I-II) and SARS-CoV-2 (III-IV) S-mediated syncytium formation on
746 293T/ACE2 cells at 48 h. f. SARS-CoV (I-II) and SARS-CoV-2 (III-IV) S-mediated
747 syncytium formation on Huh-7 cells at 48 h. Scale bar equals 400 μm in **d**-**f**.

748

749 **Fig. 2. Overall structure of post-fusion 6-HB in SARS-CoV-2.** **a**. Sequence
750 alignment of HR1 and HR2 domains in SARS-CoV and SARS-CoV-2. **b**. Structure of
751 SARS-CoV-2 6-HB is shown in cartoon representation with HR1 colored in green and
752 HR2 in cyan. The structural dimensions are indicated in angstroms. **c**. HR1 trimer of
753 SARS-CoV-2 6-HB is shown in electrostatic surface, and HR2 domain is shown in
754 cartoon representation, the important binding residues of which are shown in sticks
755 and labeled. **d**. The superposition of 6-HB structure of SARS-CoV (PDB entry
756 1WYY), MERS-CoV (PDB entry 4NJL) and SARS-CoV-2 is shown in ribbon. The
757 RMSD between structures is indicated. **e**. The sequence comparison of 6-HB structure

bioRxiv preprint doi: https://doi.org/10.1101/2020.03.09.983247. this version posted March 12, 2020. The copyright holder for this preprint (which was not certified by peer review) is the author/funder. All rights reserved. No reuse allowed without permission.

758 of different HCoVs is shown in cartoon representation with different colors for HR1
759 and HR2. The helical fusion core regions are indicated.
760
761 **Fig. 3. Interaction between HR1 and HR2 of SARS-CoV-2 and SARS-CoV. a-d**.
762 The 6-HB structure of SARS-CoV-2 and SARS-CoV is shown in cartoon
763 representation. The HR1 domain is shown in green for SARS-CoV-2 and forest for
764 SARS-CoV, while the HR2 domain is shown in cyan for SARS-CoV-2 and orange for
765 SARS-CoV. Important residues are shown in sticks and labeled.
766
767 **Fig. 4. EK1-Lipopeptides showed potent inhibitory activity against SARS-CoV-2**
768 **infection.**
769 **a**. Amino acid sequences of the designed peptides EK1 and EK1C. The dotted lines
770 represent E–K salt-bridge with i to i + 3, or i + 4 arrangement. **b**. SARS-CoV-2 S
771 protein-mediated cell-cell fusion in the presence of EK1-scramble (I), EK1 (II), EK1C
772 (III), and EK1P (IV) at 2.5 μM (scale bar: 400 μm). **c**. Inhibitory activity of
773 EK1-scramble, EK1, EK1C and EK1P against SARS-CoV-2 S-mediated cell-cell
774 fusion. **d**. Design diagram of EK1-lipopeptides with cholesterol modification,
775 including EK1C1-EK1C7. **e**. Inhibitory activity of EK1-lipopeptides on SARS-CoV-2
776 S-mediated cell-cell fusion. **f**. Inhibitory activity of EK1-lipopeptides on
777 SARS-CoV-2 PsV infection. Experiments were repeated twice, and the data are
778 expressed as means ± SD (error bar).
779

bioRxiv preprint doi: https://doi.org/10.1101/2020.03.09.983247. this version posted March 12, 2020. The copyright holder for this preprint (which was not certified by peer review) is the author/funder. All rights reserved. No reuse allowed without permission.

780 **Fig. 5. EK1C4 broadly and potently inhibited cell-cell fusion and PsV infection**
781 **mediated by S protein of divergent HCoVs. a** to **h**. Inhibitory activity of EK1C4 in
782 cell-cell fusion mediated by the S proteins of SARS-CoV (**a**), MERS-CoV (**b**),
783 HCoV-OC43 (**c**), HCoV-229E (**d**), HCoV-NL63 (**e**), WIV1 (**f**), Rs3367 (**g**) and
784 SHC014 (**h**). **i** to **o**. Inhibitory activity of EK1C4 in PsV infection assays against
785 SARS-CoV (**i**), MERS-CoV (**j**), HCoV-OC43(**k**), HCoV-229E (**l**), NL63 (**m**), WIV1
786 (**n**) and Rs3367 (**o**). Experiments were repeated twice, and the data are expressed as
787 means ± SD.
788

789 **Fig. 6. EK1C4 effectively inhibited live-CoVs infection *in vitro* and *in vivo*.**
790 **a-e.** Inhibitory activity of EK1 on live HCoV replication for SARS-CoV-2 (**a**),
791 MERS-CoV (**b**), HCoV-OC43 (**c**), HCoV-229E (**d**), and HCoV-NL63 (**e**). **f-g.** *In vivo*
792 prophylactic efficacy of EK1C4 against HCoV-OC43 infection in mice. Body weight
793 change (**f**) and survival curves (**g**) of mice challenged with HCoV-OC43. **h-i.** *In vivo*
794 therapeutic efficacy of EK1C4 against HCoV-OC43 infection in mice. Body weight
795 change (**h**) and survival curves (**i**) of mice challenged with HCoV-OC43. Experiments
796 were repeated twice, and the data are expressed as means ± SD.
797
798

bioRxiv preprint doi: https://doi.org/10.1101/2020.03.09.983247. this version posted March 12, 2020. The copyright holder for this preprint (which was not certified by peer review) is the author/funder. All rights reserved. No reuse allowed without permission.

799 **Table 1. Data collection and refinement statistics**

	SARS-CoV-2 HR1-L6-HR2 PDB entry 6LXT
Data collection	
Space group	P 1 21 1
Cell dimensions	
a, b, c (Å)	51.2, 57.6, 115.7
α, β, γ (°)	90, 91.6, 90
Wavelength (Å)	1.5418
Resolution (Å)	47.32 - 2.90 (3.00 - 2.90) †
R_{merge}	0.16 (1.13)
Mean I/σ(I)	6.3 (1.6)
Completeness (%)	95.2 (99.5)
Redundancy	7.1 (7.1)
Refinement	
Resolution (Å)	47.32 – 2.90
No. of reflections	14313
Reflections in test set	737
R_{work}/R_{free}	0.259/0.290
No. of atoms	
Protein	5205
Water & Ligands	32
r.m.s. deviations	
Bond lengths (Å)	0.013
Bond angles (°)	1.94
Ramachandran Outliers(%)	0.15
Average *B*-factor (Å^2)	87.99

800 †Highest resolution shell is shown in parenthesis.

801

802

803

804

805

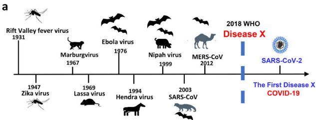
a
Rift Valley fever virus
1931
Marburgvirus
1967
Ebola virus
1976
Nipah virus
1999
MERS-CoV
2012
2018 WHO
Disease X
SARS-CoV-2
1947
Zika virus
1969
Lassa virus
1994
Hendra virus
2003
SARS-CoV
The First Disease X
COVID-19

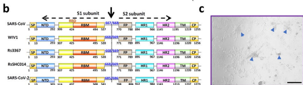
b
S1 subunit
S2 subunit
RBD
SARS-CoV
WIV1
Rs3367
RsSHC014
SARS-CoV-2
SP
NTD
RBM
FP
HR1
HR2
TM
CP
c

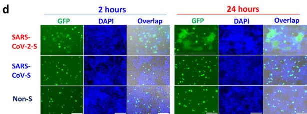
d
2 hours
24 hours
GFP
DAPI
Overlap
SARS-CoV-2-S
SARS-CoV-S
Non-S

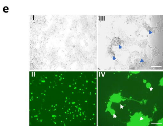
e
I
II
III
IV

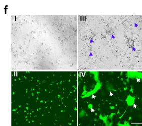
f
I
II
III
IV

a

HR1 Fusion core

S2 HR1

```
              de ga  de ga  de ga  de ga
SARS-CoV    TQNVLYENQKQIANQFNKAISQIQESLTTTSTALGKLQDVVNQNAQALNTLVKQLSSNFGAISSVLNDILSRLDKVE
SARS-CoV-2  TQNVLYENQKLIANQFNSAIGKIQDSLSSTASALGKLQDVVNQNAQALNTLVKQLSSNFGAISSVLNDILSRLDKVE
```

HR2 Fusion core

S2 HR2

```
                              de ga  de ga  de ga
SARS-CoV    DVDLGDISGINASVVNIQKEIDRLNEVAKNLNESLIDLQELGKY
SARS-CoV-2  DVDLGDISGINASVVNIQKEIDRLNEVAKNLNESLIDLQELGKY
```

b

HR1-N

HR2-C

115 Å

HR2-N

HR1-C

25 Å

c

I1198, L1197, L1193, V1189, L1186, I1183, I1179, V1177, V1176, A1174, I1172, I1169, L1166, V1164

d

SARS-CoV-2

MERS-CoV RMSD 0.66 Å

SARS-CoV RMSD 0.36 Å

e

fusion core region

SARS-CoV-2 6LXT

SARS-CoV 1WYY

MERS-CoV 4NJL

HCoV-229E 5YL9

HCoV-NL63 2IEQ

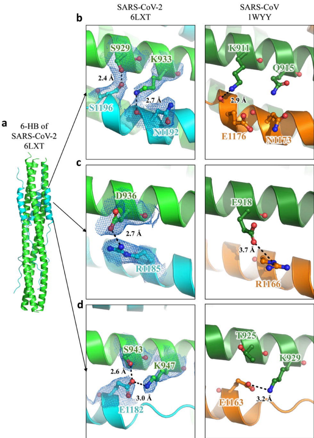
SARS-CoV-2
6LXT
SARS-CoV
1WYY
a
6-HB of
SARS-CoV-2
6LXT
b
S929
K933
2.4 Å
2.7 Å
S1196
N1192
K911
Q915
2.9 Å
E1176
N1173
c
D936
2.7 Å
R1185
E918
3.7 Å
R1166
d
S943
K947
2.6 Å
3.0 Å
E1182
T925
K929
E1163
3.2 Å

a
EK1 SLDQINVTFLDLEYEMKKLEEAIKKLEESYIDLKEL
EK1P SLDQINVTFLDLEYEMKKLEEAIKKLEESYIDLKEL-PEG4-C(Plam)
EK1C SLDQINVTFLDLEYEMKKLEEAIKKLEESYIDLKEL-PEG4-C(Chol)

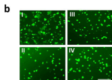
b
I
II
III
IV

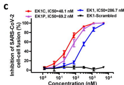
c
EK1C, IC50=48.1 nM
EK1P, IC50=69.2 nM
EK1, IC50=286.7 nM
EK1-Scrambled
Inhibition of SARS-CoV-2 cell-cell fusion (%)
Concentration (nM)

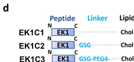
d
Peptide
Linker
Lipid
N
C
EK1C1 EK1 Chol
EK1C2 EK1 GSG Chol
EK1C3 EK1 GSG-PEG4- Chol

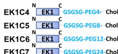
EK1C4 EK1 GSGSG-PEG4- Chol
EK1C5 EK1 GSGSG-PEG8- Chol
EK1C6 EK1 GSGSG-PEG12- Chol
EK1C7 EK1 GSGSG-PEG24- Chol

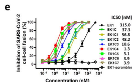
e
Inhibition of SARS-CoV-2 cell-cell fusion (%)
Concentration (nM)
IC50 (nM)
EK1 315.0
EK1C 37.3
EK1C1 56.8
EK1C2 48.2
EK1C3 10.6
EK1C4 1.3
EK1C5 3.1
EK1C6 3.9
EK1C7 3.9
EK1-scrambled

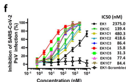
f
Inhibition of SARS-CoV-2 PsV infection (%)
Concentration (nM)
IC50 (nM)
EK1 2375.0
EK1C 139.4
EK1C1 480.3
EK1C2 418.6
EK1C3 86.4
EK1C4 15.8
EK1C5 31.3
EK1C6 77.4
EK1C7 84.4
EK1-Scrambled

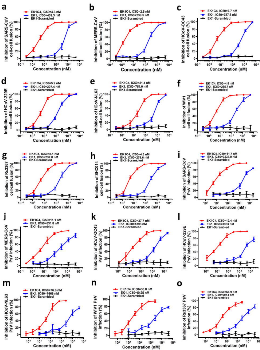
a
EK1C4, IC50=4.3 nM
EK1, IC50=409.3 nM
EK1-Scrambled
Inhibition of SARS-CoV cell-cell fusion (%)
Concentration (nM)
b
EK1C4, IC50=2.5 nM
EK1, IC50=239.5 nM
EK1-Scrambled
Inhibition of MERS-CoV cell-cell fusion (%)
Concentration (nM)
c
EK1C4, IC50=7.7 nM
EK1, IC50=787.6 nM
EK1-Scrambled
Inhibition of HCoV-OC43 cell-cell fusion (%)
Concentration (nM)
d
EK1C4, IC50=5.2 nM
EK1, IC50=207.4 nM
EK1-Scrambled
Inhibition of HCoV-229E cell-cell fusion (%)
Concentration (nM)
e
EK1C4, IC50=21.4 nM
EK1, IC50=751.0 nM
EK1-Scrambled
Inhibition of HCoV-NL63 cell-cell fusion (%)
Concentration (nM)
f
EK1C4, IC50=4.5 nM
EK1, IC50=265.7 nM
EK1-Scrambled
Inhibition of WIV1 cell-cell fusion (%)
Concentration (nM)
g
EK1C4, IC50=8.1 nM
EK1, IC50=237.0 nM
EK1-Scrambled
Inhibition of Rs3367 cell-cell fusion (%)
Concentration (nM)
h
EK1C4, IC50=4.3 nM
EK1, IC50=279.6 nM
EK1-Scrambled
Inhibition of SHC014 cell-cell fusion (%)
Concentration (nM)
i
EK1C4, IC50=11.7 nM
EK1, IC50=3237.0 nM
EK1-Scrambled
Inhibition of SARS-CoV PsV infection (%)
Concentration (nM)
j
EK1C4, IC50=11.1 nM
EK1, IC50=631.8 nM
EK1-Scrambled
Inhibition of MERS-CoV PsV infection (%)
Concentration (nM)
k
EK1C4, IC50=37.7 nM
EK1, IC50=1398 nM
EK1-Scrambled
Inhibition of HCoV-OC43 PsV infection (%)
Concentration (nM)
l
EK1C4, IC50=12.4 nM
EK1, IC50=3963 nM
EK1-Scrambled
Inhibition of HCoV-229E PsV infection (%)
Concentration (nM)
m
EK1C4, IC50=76.6 nM
EK1, IC50=7666 nM
EK1-Scrambled
Inhibition of HCoV-NL63 PsV infection (%)
Concentration (nM)
n
EK1C4, IC50=30.8 nM
EK1, IC50=5425 nM
EK1-Scrambled
Inhibition of WIV1 PsV infection (%)
Concentration (nM)
o
EK1C4, IC50=66.9 nM
EK1, IC50=6014 nM
EK1-Scrambled
Inhibition of Rs3367 PsV infection (%)
Concentration (nM)

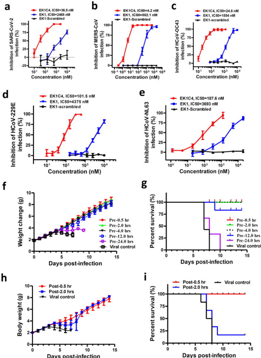
a
EK1C4, IC50=36.5 nM
EK1, IC50=2468 nM
EK1-Scrambled
Inhibition of SARS-CoV-2 infection (%)
Concentration (nM)
b
EK1C4, IC50=4.2 nM
EK1, IC50=802.1 nM
EK1-Scrambled
Inhibition of MERS-CoV infection (%)
Concentration (nM)
c
EK1C4, IC50=24.8 nM
EK1, IC50=1554 nM
EK1-scrambled
Inhibition of HCoV-OC43 infection (%)
Concentration (nM)
d
EK1C4, IC50=101.5 nM
EK1, IC50=4375 nM
EK1-scrambled
Inhibition of HCoV-229E infection (%)
Concentration (nM)
e
EK1C4, IC50=187.6 nM
EK1, IC50=3693 nM
EK1-Scrambled
Inhibition of HCoV-NL63 infection (%)
Concentration (nM)
f
Weight change (g)
Pre-0.5 hr
Pre-2.0 hrs
Pre-4.0 hrs
Pre-12.0 hrs
Pre-24.0 hrs
Viral control
Days post-infection
g
Percent survival (%)
Pre-0.5 hr
Pre-2.0 hrs
Pre-4.0 hrs
Pre-12.0 hrs
Pre-24.0 hrs
Viral control
Days post-infection
h
Body weight (g)
Post-0.5 hr
Post-2.0 hrs
Viral control
Days post-infection
i
Percent survival (%)
Post-0.5 hr
Post-2.0 hrs
Viral control
Days post-infection